The Plant Cell, Vol. 32: 1270–1284, April 2020, www.plantcell.org © 2020 ASPB.

Arabidopsis *KETCH1* Is Critical for the Nuclear Accumulation of Ribosomal Proteins and Gametogenesis

Feng Xiong,[a,1] Cun-Ying Duan,[a,1] Hai-Hong Liu,[a] Ju-Hua Wu,[a] Zhong-Hui Zhang,[c] Sha Li,[a,b,2] and Yan Zhang[a,2]

[a] State Key Laboratory of Crop Biology, College of Life Sciences, Shandong Agricultural University, Tai'an 271018, China
[b] Department of Plant Biology and Ecology, College of Life Sciences, Nankai University, Tianjin 300071, China
[c] Guangdong Provincial Key Laboratory of Biotechnology for Plant Development, School of Life Science, South China Normal University, Guangzhou 510631, China

ORCID IDs: 0000-0002-6434-4588 (F.X.); 0000-0003-2005-8261 (C.-Y.D.); 0000-0003-3797-4602 (H.-H.L.); 0000-0002-7578-0844 (J.-H.W.); 0000-0003-3732-8010 (Z.-H.Z.); 0000-0002-7197-0181 (S.L.); 0000-0002-3501-5857 (Y.Z.)

Male and female gametophytes are generated from micro- or megaspore mother cells through consecutive meiotic and mitotic cell divisions. Defects in these divisions often result in gametophytic lethality. Gametophytic lethality was also reported when genes encoding ribosome-related proteins were mutated. Although numerous ribosomal proteins (RPs) have been identified in plants based on homology with their yeast and metazoan counterparts, how RPs are regulated, e.g., through dynamic subcellular targeting, is unknown. We report here that an Arabidopsis (*Arabidopsis thaliana*) importin β, KETCH1 (karyopherin enabling the transport of the cytoplasmic HYL1), is critical for gametogenesis. Karyopherins are molecular chaperones mediating nucleocytoplasmic protein transport. However, the role of KETCH1 during gametogenesis is independent of HYPONASTIC LEAVES 1 (HYL1), a previously reported KETCH1 cargo. Instead, KETCH1 interacts with several RPs and is critical for the nuclear accumulation of RPL27a, whose mutations caused similar gametophytic defects. We further showed that knocking down *KETCH1* caused reduced ribosome biogenesis and translational capacity, which may trigger the arrest of mitotic cell cycle progression and lead to gametophytic lethality.

Introduction

Development of gametophytes is critical for plant reproduction. In angiosperms, megagametogenesis (Drews and Yadegari, 2002) and microgametogenesis (McCormick, 1993, 2004) produce female and male gametophytes, respectively. During megagametogenesis, meiosis of a megaspore mother cell (MMC) produces four megaspores, among which only one survives as a functional megaspore (FM). The FM undergoes three rounds of mitosis and cellularization to develop into an embryo sac, i.e., the female gametophyte (Drews and Yadegari, 2002). During microgametogenesis, meiosis of a microspore mother cell gives rise to a tetrad of microspores. After release from the tetrad, each microspore goes through an asymmetric cell division, referred to as pollen mitosis I (PMI), to produce a bicellular microspore containing a generative cell and a vegetative nucleus. The generative cell then undergoes another mitotic event, called pollen mitosis II, to produce two sperm cells enclosed in pollen together with the vegetative nucleus (McCormick, 1993, 2004).

Mutations of mitotic cell cycle regulators often impair gametogenesis (Liu and Qu, 2008). Cyclin-dependent kinase (CDK)-activating kinases CDKD;1 and CDKD;3 are essential for preserving mitotic activity in Arabidopsis (*Arabidopsis thaliana*), and double mutants with defects in both of these proteins showed gametophytic lethality due to defective mitosis (Takatsuka et al., 2015). Similarly, the triple mutant of CDK, *cdka;1/+*;*cdkb1;1*;*cdkb1;2*, was defective in male and female gametogenesis due to mitotic division defects (Nowack et al., 2012). Two RING-finger E3 ligases, RING-H1 group F1a (RHF1a) and RHF2a, interact and target a CDK inhibitor ICK4/KRP6 for degradation (Liu et al., 2008). Mutants of the E3 ligase pair resulted in interphase arrest of the mitotic cell cycle at the microspore stage of pollen development and at female gametogenesis (FG) stage 1 of embryo sac development, leading to male and female gametophytic lethality (Liu et al., 2008).

The other major class of genes whose mutations may cause gametophytic lethality encodes proteins involved in ribosome biogenesis. In Arabidopsis, RIBOSOMAL PROTEIN L10 (RPL10; Imai et al., 2008; Falcone Ferreyra et al., 2010, 2013), RPL27a (Szakonyi and Byrne, 2011; Zsögön et al., 2014), SLOW WALKER1 (SWA1; Shi et al., 2005), SWA2 (Li et al., 2009), and two DEAD-box RNA helicases, AtRH36 (Huang et al., 2010) and SWA3 (Liu et al., 2010), are likely required for the biogenesis of rRNAs, the export of preribosomes from the nucleus, or the biogenesis of ribosomes. Mutations at these genes all resulted in mitotic arrest during gametogenesis (Shi et al., 2005; Imai et al., 2008; Li et al., 2009; Falcone Ferreyra et al., 2010, 2013; Huang et al., 2010; Liu et al., 2010). Although these results demonstrated the importance of RPs and their associated proteins, how these proteins are regulated, such as via dynamic targeting, is poorly understood.

Karyopherins, more often known as importins or exportins, are molecular chaperones mediating the nucleocytoplasmic transport of proteins (Meier and Brkljacic, 2009; Tamura and Hara-Nishimura, 2014). Classic nucleocytoplasmic transport relies on importin α for recognizing nuclear localization signals (NLSs) and

[1] These authors contributed equally to this work.
[2] Address correspondence to yzhang@sdau.edu.cn and shali@sdau.edu.cn
The authors responsible for distribution of materials integral to the findings presented in this article in accordance with the policy described in the Instructions for Authors (www.plantcell.org) are: Yan Zhang (yzhang@sdau.edu.cn) and Sha Li (shali@sdau.edu.cn).
www.plantcell.org/cgi/doi/10.1105/tpc.19.00791

importin β for interacting with the nuclear pore complex (NPC) and Ran-GTP (Tamura and Hara-Nishimura, 2014). However, importin βs play diverse roles, such as in the assembly of the mitotic spindle, in nuclear membrane formation, in microRNA activities, and in maintaining protein stability (Harel and Forbes, 2004; Wang et al., 2011; Tamura and Hara-Nishimura, 2014; Cui et al., 2016; Liu et al., 2019).

We report here that an Arabidopsis importin β, KETCH1 (KARYOPHERIN ENABLING THE TRANSPORT OF THE CYTOPLASMICHYL1), is critical for male gametogenesis and FG. Functional loss of *KETCH1* caused the arrest of male gametophytic development at PMI and of female gametophytic development at FG1, suggesting a key role of KETCH1 in mitotic progression during gametogenesis. We demonstrate that the role of KETCH1 during gametogenesis is independent of HYPONASTIC LEAVES 1 (HYL1), the previously reported KETCH1 cargo. We show that KETCH1 interacts with a few ribosomal proteins (RPs), including RPL27a, whose nuclear accumulation depends on KETCH1 and whose mutations caused similar gametophytic defects. Knocking down *KETCH1* resulted in reduced translational capacity, which may trigger mitotic arrest.

Results

Functional Loss of *KETCH1* Compromises Male and Female Transmission

Arabidopsis *KETCH1* encodes an importin β (Tamura and Hara-Nishimura, 2014). It was reported previously that mutations of *KETCH1* resulted in embryo lethality, and thus no homozygous mutants of *KETCH1* could be obtained (Zhang et al., 2017). However, compared to the full seed set in the wild type (Figures 1A and 1K), the heterozygous mutant of *KETCH1*, *ketch1-2*/+, contained around 47% tiny and wrinkled ovules (Figures 1B and 1K), much higher than 25% as expected for embryo lethality. As there were a higher number of aborted seeds, we decided to investigate if the mutation affected gametophyte development. Wild-type ovules at 24 h after pollination (HAP) were fertilized and showed developing embryo and endosperm by whole-mount clearing and optical sections of pistils (Figures 1G and 1H). By contrast, the small and wrinkled ovules in *ketch1-2*/+ were unfertilized, containing irregularly distributed nuclei (Figures 1I and 1J), suggesting a female gametophytic defect of *ketch1-2*. Indeed, when *ketch1-2*/+ was used as the female parent in reciprocal crosses with wild type, seed set was severely reduced (Figures 1C, 1D, and 1K), further supporting a role of *KETCH1* in female gametophytic functionality. By analyzing the progenies of such crosses, we determined that both male and female gametophytic transmissions of *ketch1-2* were severely reduced (Table 1), suggesting that *KETCH1* is critical for male gametogenesis and FG, in addition to its roles in embryogenesis (Zhang et al., 2017).

Male Gametophytic Development Is Defective in *KETCH1* Loss-of-Function Mutants

To determine the cause of reduced male transmission (Table 1), we performed Alexander staining to analyze cytoplasmic viability, DAPI staining to examine nuclear structure, and SEMs to examine pollen morphology. Compared to wild-type pollen grains that were stained purple by Alexander dye (Figures 2A, 2C, and 2K), 33.9%

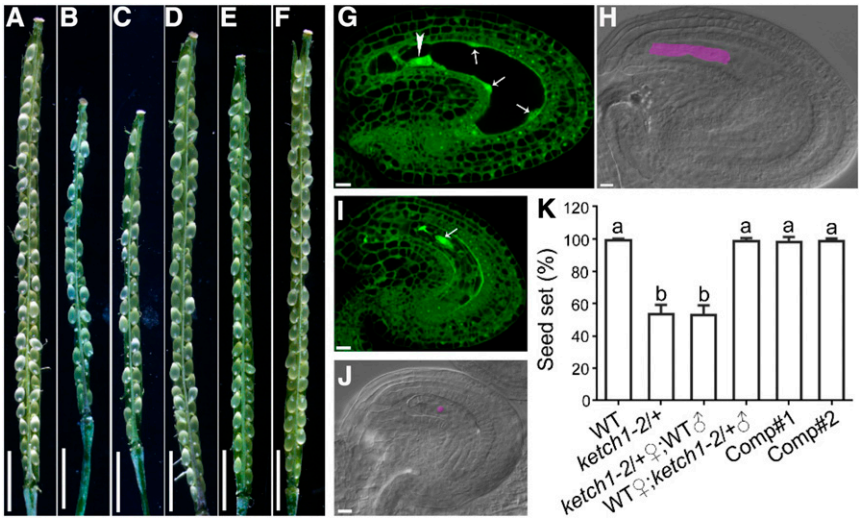

Figure 1. Reduced Seed Set in *ketch1*/+ Was Due to Female Gametophytic Defect.

(A) to **(F)** A representative silique from self-fertilized wild type **(A)** or *ketch1-2*/+ **(B)**, from *ketch1-2*/+ pistil pollinated with wild-type pollen **(C)** or wild-type pistil pollinated with *ketch1-2*/+ pollen **(D)** or from two complementation lines, i.e., Pro_{UBQ10}:KETCH1-YFP;*ketch1-2* **(E)** and **(F)**.
(G) to **(J)** Optical sections **(G)** and **(I)** or whole-mount clearing **(H)** and **(J)** of wild-type **(G)** and **(H)** or *ketch1-2* **(I)** and **(J)** ovules pollinated with wild-type pollen at 24 HAP. Arrows in **(G)** point at initiating peripheral endosperm; the arrowhead in **(G)** points at the nucleus of the zygote; the arrow in **(I)** points at the single nucleus in the embryo sac. Region highlighted in lilac is an elongated zygote in wild type **(H)** or the single nucleus in the abnormal embryo sac of *ketch1-2* **(J)**.
(K) Seed set. Results shown are means ± SD (n = 50 to 100). Means with different letters indicate significant difference (one-way ANOVA, Tukey's multiple comparison test, $P < 0.05$). Bars = 2 mm for **(A)** to **(F)**; 10 μm for **(G)** to **(J)**.

Table 1. Transmission of Both Male and Female Is Defective by *KETCH1* Loss of Function

Parents	Genotype of Progenies				
	KETCH1	*ketch1-2*/+	*ketch1-2*	Observed Ratio	Expected Ratio
♀*ketch1-2*/+ ×♂wild type	105	60	0	1:0.57[a]	1:1
♀wild type ×♂*ketch1-2*/+	60	30	0	1:0.50[a]	1:1
♀*ketch1-2*/+ ×♂*ketch1-2*/+	77	115	0	1:1.49:0[b]	1:2:1

[a]Significantly different from the expected segregation ratio 1:1 ($\chi^2 < \chi^2_{0.05,1}$).
[b]Significantly different from the expected segregation ratio 1:2:1 ($\chi^2 < \chi^2_{0.05,2}$).

pollen from the *ketch1-2*/+ plants were light blue (Figures 2B, 2D, and 2K), indicating pollen abortion. In wild type, mature pollen grains stained with DAPI showed two sperm nuclei and one vegetative nucleus (Figures 2E, 2K, and 2L), whereas 30% pollen from the *ketch1-2*/+ plants failed to show nuclei at all (Figures 2F, 2K, and 2L). Finally, SEMs of the wild type showed oval-shaped pollen grains (Figures 2G, 2I, and 2M), whereas 32% pollen from *ketch1-2*/+ were wrinkled or collapsed (Figures 2H, 2J, and 2M). These results suggest that *KETCH1* is critical for the development of male gametophytes, i.e., pollen.

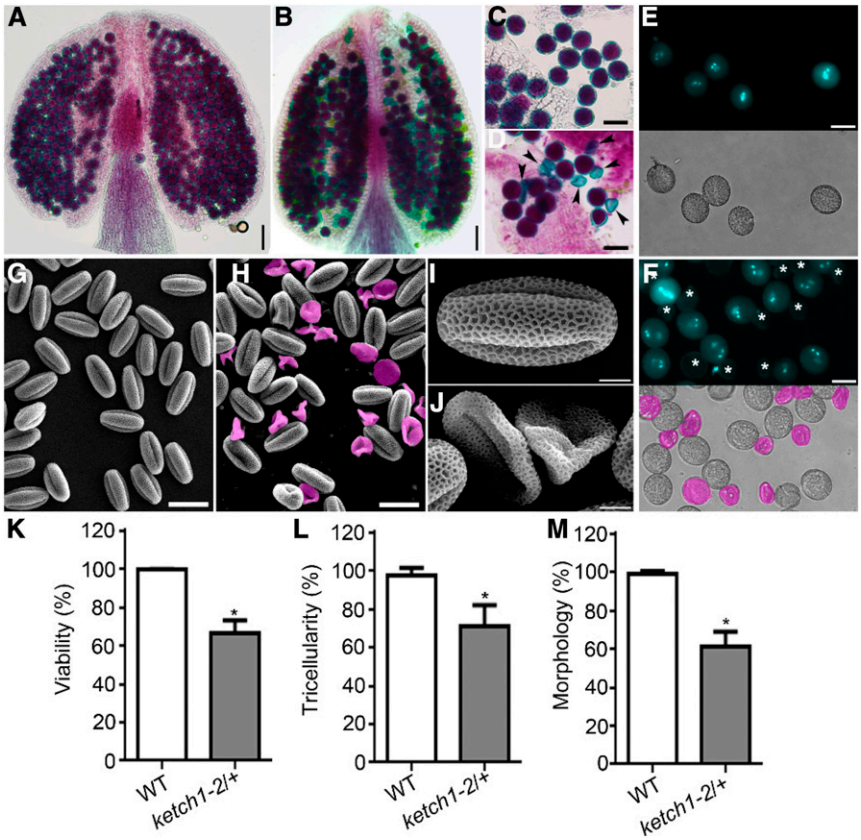

Figure 2. Pollen Development Was Defective in *KETCH1* Loss-of-Function Mutants.

(A) to **(D)** Alexander staining of a representative anther **(A)** and **(B)** or mature pollen grains **(C)** and **(D)** from wild type **(A and C)** or *ketch1-2*/+ **(B)** and **(D)**. Arrowheads point at aborted pollen grains.

(E) and **(F)** DAPI staining of mature pollen grains from wild type **(E)** or *ketch1-2*/+ **(F)**. Bright-field (BF) images are shown at the bottom of corresponding fluorescent images. Aborted pollen grains are labeled by asterisks (in the fluorescent image) or in pink (in the BF image).

(G) to **(J)** Scanning electron micrographs (SEMs) of mature pollen from wild type **(G)** and **(I)** or *ketch1-2*/+ **(H)** and **(J)**. Aborted pollen grains are highlighted in pink.

(K) to **(M)** Percentage of viable pollen by Alexander staining **(K)** of pollen with tricellular structure by DAPI staining **(L)** or of oval-shaped pollen by SEM **(M)**. Results shown are means ± SD ($n = 50$ to 100). Asterisks indicate a significant difference of *ketch1-2*/+ from wild type (*t* test, $P < 0.05$). Bars = 50 μm for **(A)** and **(B)**; 25 μm for **(C)**, **(D)**, **(G)**, and **(H)**; 20 μm for **(E)** and **(F)**; 5 μm for **(I)** and **(J)**.

To provide further evidence that *ketch1-2* pollen was defective, we introduced *quartet1* (*qrt1*) into *ketch1-2*/+. In *qrt1*, the four pollen grains of microsporogenesis remain fused and thus make genetic analysis of a heterozygous plant easier (Francis et al., 2006). In *qrt1*, the majority of tetrads had four or three pollen tubes during in vitro germination assays (Supplemental Figure 1). By contrast, the majority of tetrads in *ketch1-2*/+;*qrt1* only had one or two pollen tubes (Supplemental Figure 1). These results suggest that functional loss of *KETCH1* compromises gametophytic pollen development.

KETCH1 Loss of Function Impairs PMI

To determine at which stage the development of *ketch1-2* pollen started to be defective, we analyzed anthers at different developmental stages by plastic embedding and semithin transverse sections. Anther development in Arabidopsis is classified into 14 stages (Sanders et al., 1999), which correspond to specific pollen developmental stages (Borg et al., 2009). Pollen development seems comparable between wild type and *ketch1-2*/+ before stage 10 (Figure 3A), i.e., the stage of unicellular microspore (Borg et al., 2009). At stage 11, the unicellular microspore in wild type undergoes one round of mitosis, i.e., PMI, to produce a bicellular microspore (Borg et al., 2009). This event accompanied the conversion of large vacuoles into numerous small ones in wild type (Figure 3A), as previously reported (Yamamoto et al., 2003). By contrast, some microspores in *ketch1-2*/+ pollen were deformed, containing large vacuoles at stage 11 (Figure 3A). At maturation, debris of aborted pollen grains was detected in *ketch1-2*/+ anther, alongside normally developed ones (Figure 3A). To confirm the results by plastic sections, we examined floral buds containing unicellular or bicellular microspores (Supplemental Figure 2) for optical sections by confocal laser scanning microscopy (CLSM) as described (Zhang et al., 2018). Consistent with the results obtained by plastic sections, CLSM showed microspores containing large vacuoles at stage 11 in *ketch1-2*/+ anthers in contrast to those of wild type (Supplemental Figure 2).

To provide a detailed histological analysis of pollen developmental defects in *ketch1-2*/+, we performed ultrastructural analysis of *ketch1-2*/+ anthers using transmission electron microscopy (TEM). At stage 11, a portion of microspores in *ketch1-2*/+ anthers showed normal intracellular morphology, i.e., contained a vegetative nucleus, a generative cell nucleus, and numerous small vacuoles (Figure 3B). Others, however, showed similar defects, albeit to a different extent (Figures 3C to 3E). These microspores contained only one nucleus and few large vacuoles (Figures 3C to 3E). At early stages, the PM of these microspores was invaginated and wrinkled (Figure 3C). In these microspores, the single nucleus was abnormally surrounded by vacuolar structures (Figure 3C). Later on, defects appeared more obvious, such that the PM was detached from cell wall (Figure 3D) and finally degenerated together with the cytoplasm and the nucleus (Figure 3E). Results from TEM indicate that *ketch1-2* microspores are defective during PMI, which is detrimental to pollen development.

KETCH1 Loss-of-Function Results in the Mitotic Arrest of FMs

To characterize the defects in *ketch1-2* female gametophytes (Table 1), we examined *ketch1-2*/+ ovules at different developmental stages by optical sections through CLSM (Wang et al., 2016). In wild type, FM persisted among the three degenerating sisters from MMC at stage 3-I (Figure 4A). At this stage, *ketch1-2* was comparable to wild type (Figures 4A and 4B). Later on, FM

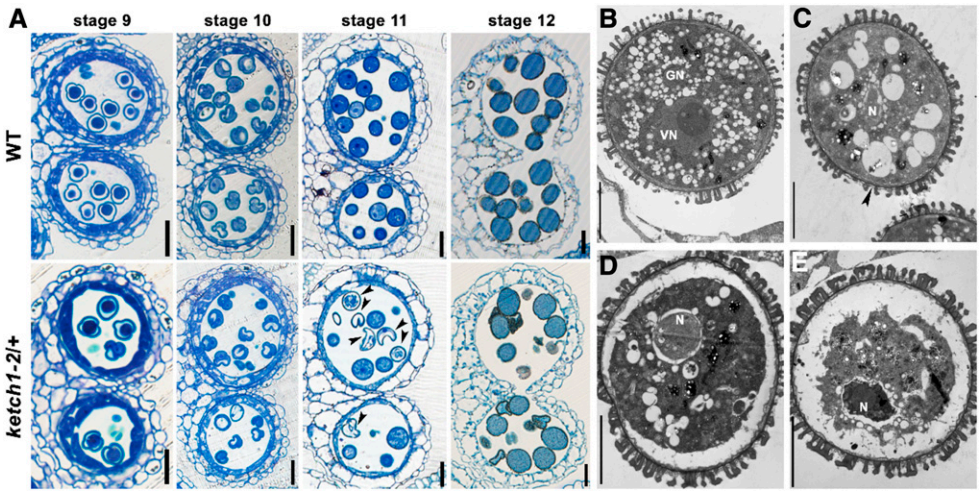

Figure 3. *KETCH1* Loss-of-Function Compromised PMI during Pollen Development.

(A) Representative semithin transverse sections of developing anthers at stage 9, stage 10, stage 11, or stage 12 from wild type or *ketch1-2*/+. Arrowheads point at aborted microspores.

(B) to **(E)** Representative TEM sections of *ketch1-2*/+ anthers at stage 11, showing a wild-type-looking microspore **(B)** and defective microspores at early **(C)**, middle **(D)**, or late **(E)** stages. Arrowhead in **(C)** points at invaginated PM. N, Nucleus; GN, generative nucleus; VN, vegetative nucleus. Bars = 20 μm for **(A)**; 5 μm for **(B)** to **(E)**.

underwent three rounds of mitotic cell division to produce the embryo sac (Figure 4A). At maturation, an embryo sac contains a central cell, an egg cell, and two synergid cells (Figure 4A). By contrast, almost 30% ovules in *ketch1-2*/+ did not contain a mature embryo sac (Figure 4B). Although all stage 3-I ovules in *ketch1-2*/+ contained a FM, FM in some ovules failed to go through the first mitotic division (Figure 4B). As a consequence, these ovules at stage 3-III did not contain two nuclei as in wild type (Figures 4A and 4C) but one FM (Figures 4B and 4C). In these ovules, integument growth was not affected and thus provided the information for developmental stages (Figure 4B). As a consequence of failed mitosis of FM, in 30% mature ovules of *ketch1-2*/+, the embryo sac contained irregular numbers of nuclei, ranging from one to six (Figures 4B and 4C). Indeed, by introducing an egg cell-specific reporter construct Pro_{DD45}:β-glucuronidase (GUS; Steffen et al., 2007; Wang et al., 2016), we found that a portion of mature ovules in *ketch1-2*/+ pistils did not show GUS signals (Figure 4E) in comparison to that in wild type (Figure 4D). In addition, the embryo sac-specific promoter-driven nucleus-targeted yellow fluorescent protein (YFP), i.e., Pro_{ES1}:NLS-YFP (Wang et al., 2017), showed seven nuclei in wild-type ovules (Figure 4F). By contrast, 36 out of 156 ovules from Pro_{ES1}:NLS-YFP;*ketch1-2*/+

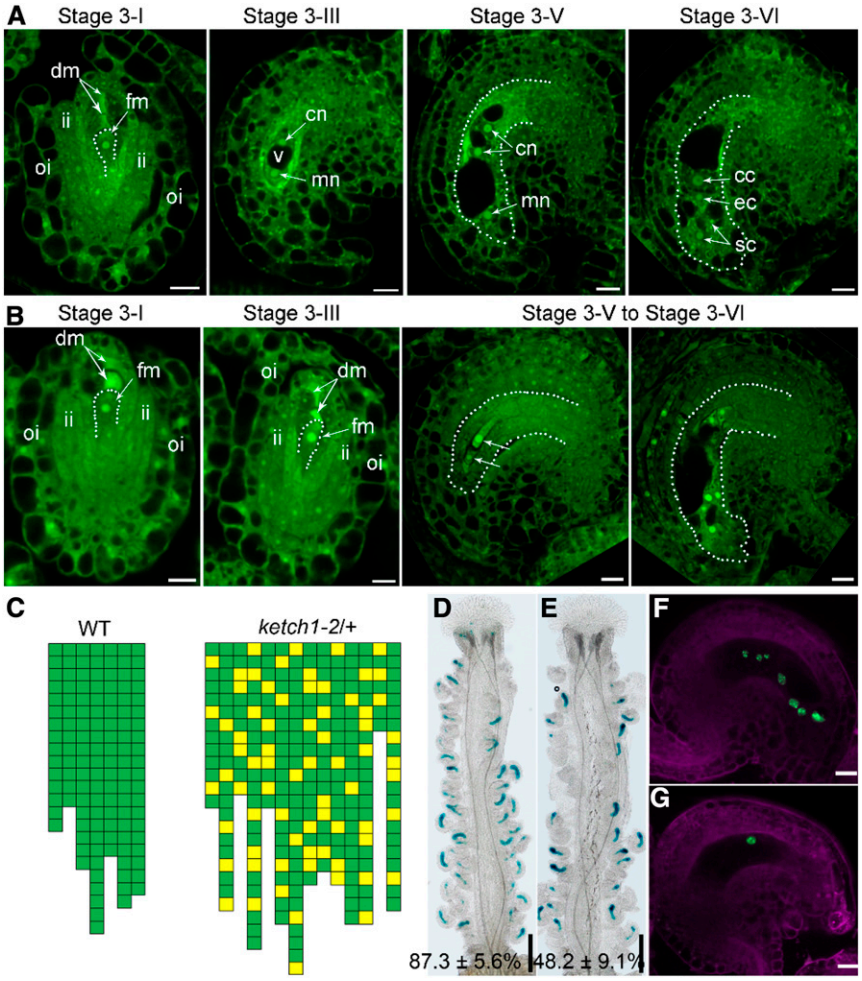

Figure 4. *KETCH1* Loss of Function Resulted in the Defective Development of Female Gametophytes.

(A) and **(B)** CLSMs of representative wild-type **(A)** or *ketch1-2* **(B)** ovules during development. Dotted lines either illustrate functional megaspore (FM) of stage 3-I ovules or the embryo sac of ovules at other stages. cc, Central cell; cn, chalazal nucleus; dm, degenerating megaspore; ec, egg cell; fm, functional megaspore; ii, inner integument; mn, micropylar nucleus; oi, outer integument; sc, synergid cell.

(C) Quantification of embryo sac development based on CLSM of mature ovules. Each column represents one mature pistil; the number of cubes in each column indicates the number of countable ovules; green cubes indicate embryo sacs with normal seven-nucleus structure, whereas yellow cubes indicate abnormal embryo sacs as shown in **(B)**. The positions of yellow squares indicate their positions in the pistils.

(D) and **(E)** Representative histochemical GUS staining of pistils from Pro_{DD45}:GUS **(D)** or from Pro_{DD45}:GUS;*ketch1-2*/+ transgenic plants **(E)**. Values shown at the bottom (% of GUS-positive ovules) are means ± SD ($n = 20$). The *ketch1-2*/+ mutant is significantly different from wild type (*t* test, $P < 0.05$).

(F) and **(G)** Overlaid CLSM images of lysotracker red (magenta)-stained Pro_{ES1}:NLS-YFP **(F)** or Pro_{ES1}:NLS-YFP; *ketch1-2*/+ transgenic plants **(G)**. Bars = 200 μm for **(D)** and **(E)**; 10 μm for **(A)**, **(B)**, **(F)**, and **(G)**.

showed only one nucleus (Figure 4G). These results show that *KETCH1* is critical for the mitotic cell division of FM during megagametogenesis.

To provide further support of the roles *KETCH1* plays in gametogenesis, we generated transgenic lines down-regulating *KETCH1* specifically during gametogenesis using a gametophytic-specific promoter Pro_{GPR1} (Yang et al., 2017). The expression of KETCH1-RNAi by Pro_{GPR1} caused pollen abortion and reduced female fertility (Supplemental Figure 3), just like those by *KETCH1* loss of function.

We suspected that the reduced seed set in the heterozygous *ketch1-2*/+ was due to defective embryo sacs. To test this hypothesis, we pollinated wild-type or *ketch1-2*/+ pistils by Pro_{LAT52}:GUS or by wild-type pollen and examined pistils at 12 HAP or 48 HAP, respectively. At 12 HAP, the majority of wild-type ovules were targeted by one pollen tube, as shown by SEM (Figure 5A) or by histochemical GUS staining of pistils (Figure 5C). In comparison, around 35% ovules in *ketch1-2*/+ failed to attract a pollen tube (Figure 5D). In these ovules, a pollen tube exited the transmission track and grew along the funiculus (Figure 5B). However, it failed to enter the micropyle (Figures 5B and 5D). At 48 HAP, wild-type ovules were fertilized and showed rapid size increase (Figure 5E). By contrast, more than 35% ovules in *ketch1-2*/+ remained tiny due to failed fertilization (Figure 5F). These results demonstrate that defective embryo sac development by *KETCH1* loss of function compromises pollen tube guidance and thus causes reduced female fertility.

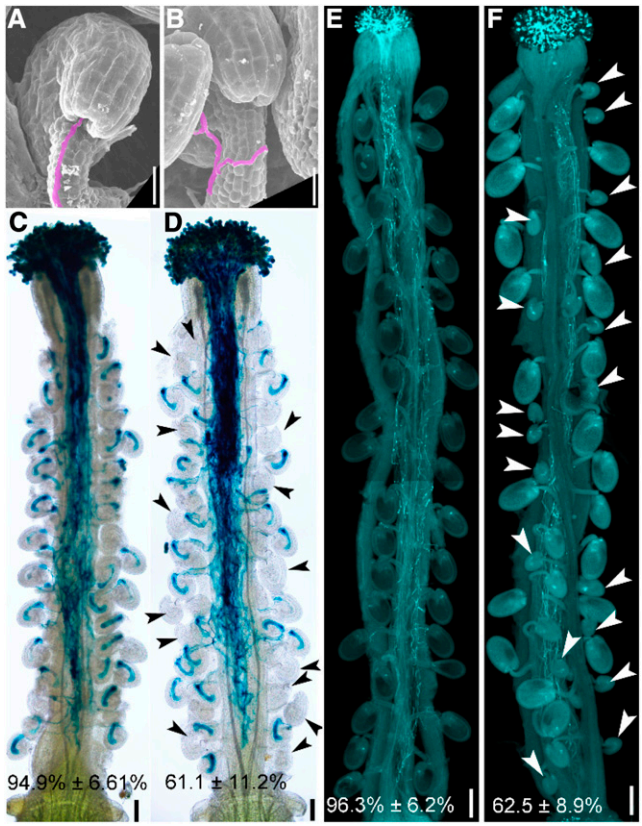

Figure 5. *KETCH1* Loss of Function Compromised Pollen Tube Guidance.

(A) and **(B)** SEMs of a wild-type **(A)** or a *ketch1-2*/+ ovule **(B)** pollinated with wild-type pollen at 12 HAP. Pollen tubes are shown in lilac.

(C) and **(D)** Histochemical GUS staining of a wild-type **(C)** or a *ketch1-2*/+ pistil **(D)** pollinated with Pro_{LAT52}:GUS pollen at 12 HAP. Two overlapping high-magnification images were taken for one pistil. The images were then overlaid with Photoshop (Adobe) to show the whole pistil. Arrowheads point at the ovules not targeted by a pollen tube.

(E) and **(F)** Aniline blue staining of a wild-type **(E)** or a *ketch1-2*/+ pistil **(F)** pollinated with wild-type pollen at 48 HAP. Arrowheads in **(F)** point at unfertilized ovules. Results shown at the bottom of **(C)** to **(F)** are means ± SD ($n = 20$). The *ketch1-2*/+ mutant is significantly different from wild type (*t* test, $\mathbf{P} < 0.05$). Bars = 20 μm for **(A)** and **(B)**; 100 μm for **(C)** and **(D)**; 200 μm for **(E)** and **(F)**.

Expression and Subcellular Localization of KETCH1

KETCH1 is highly expressed in reproductive tissues such as inflorescence, ovules, and pollen by quantitative RT-PCRs (Supplemental Figure 4). Analysis of *KETCH1* promoter-driven GUS reporter lines, Pro_{KETCH1}:GUS, verified the enriched expression of *KETCH1* in reproductive tissues/cells (Supplemental Figure 4). To provide further evidence that *KETCH1* was critical for PMI during pollen development and mitosis of FM, we examined its expression specifically in these processes. A *KETCH1* promoter-driven nuclear-localized YFP (Pro_{KETCH1}:NLS-YFP) was generated, and CLSM imaging was performed with 10 lines of Pro_{KETCH1}:NLS-YFP transgenic plants. During pollen development, signals were detected strongly in unicellular and bicellular microspores (Figures 6B and 6C) but hardly at the tetrad stage (Figure 6A) or in tricellular pollen (Figure 6D). During ovule development, signals were first detected in MMC and initiating integument cells (Figure 6E). At stage 2-III, signals were detected in FM in addition to integument (Figure 6G). At later stages, the promoter of *KETCH1* was active in the nuclei of developing embryo sac (Figures 6F, 6H, and 6I). These results show that *KETCH1* is expressed during gametogenesis.

To examine the subcellular localization of KETCH1, we generated Pro_{UBQ10}:KETCH1-YFP. The YFP translational fusion driven by Pro_{UBQ10} rescued the male and female gametophytic defects of *ketch1-2* (Figures 1E, 1F, and 1K; Supplemental Figure 5), indicating that GFP fusion did not interfere with the functionality of KETCH1. By CLSM, it was shown that KETCH1 was distributed both in the nucleus and in the cytoplasm either in ovules, in microspores, or in roots (Supplemental Figure 6), as reported (Zhang et al., 2017).

Functional Loss of *HYL1* Did Not Affect Gametogenesis

KETCH1 was reported to mediate the nucleocytoplasmic transport of HYPONASTIC LEAVES 1 (HYL1; Zhang et al., 2017), a miRNA regulator (Lu and Fedoroff, 2000; Vazquez et al., 2004). Although the null mutant of *HYL1*, i.e., *hyl1-2*, was reported to show reduced fertility (Vazquez et al., 2004), both male and female gametophytic transmission of *hyl1-2* were comparable to those of wild type (Supplemental Table 1), suggesting that compromised nucleocytoplasmic transport of HYL1 is not responsible for KETCH1 function during gametogenesis.

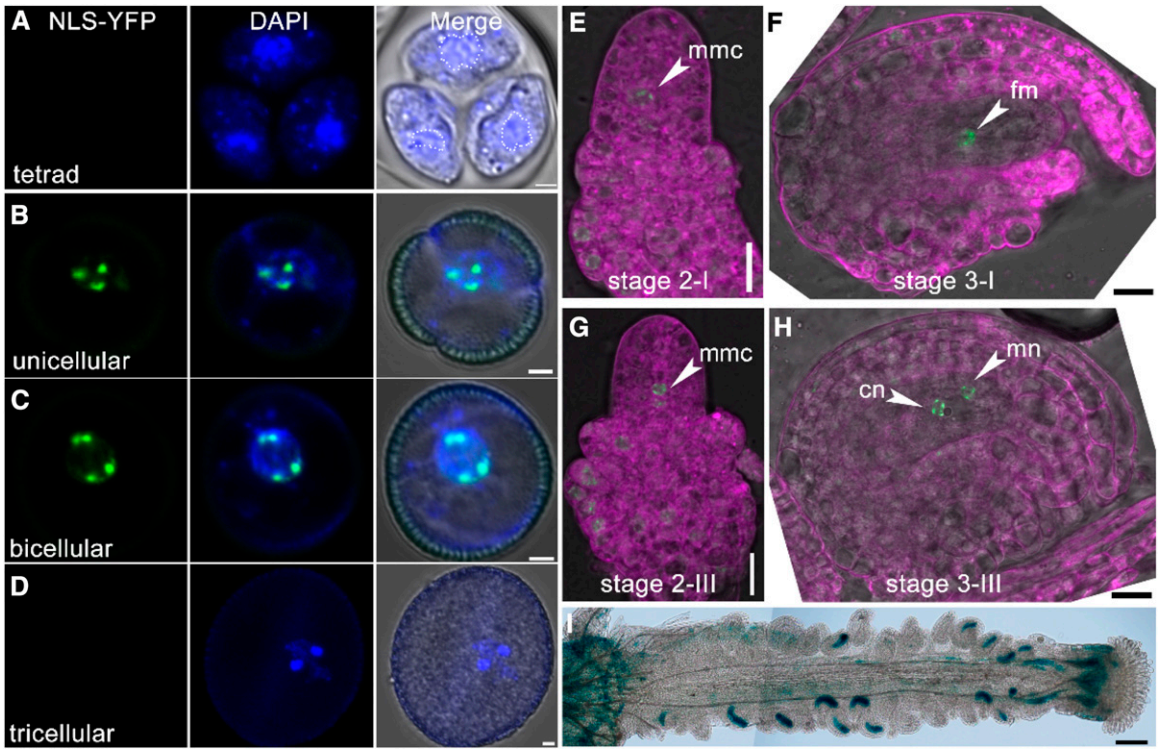

Figure 6. *KETCH1* Is Expressed in Reproductive Cells.

(A) to **(H)** CLSM of Pro_{KETCH1}:NLS-YFP in developing microspores at tetrad **(A)**, unicellular **(B)**, bicellular **(C)**, tricellular microspores **(D)**, and ovules at stage 2-I **(E)**, stage 2-III **(G)**, stage 3-I **(F)**, and stage 3-III ovules **(H)**. Dotted lines in **(A)** illustrate vegetative nuclei. Images in **(E)** to **(H)** are merges of the RFP (for lysotracker red staining, in magenta), YFP (for NLS-YFP, green), and transmission channels.
(I) Histochemical GUS staining of a mature Pro_{KETCH1}:GUS pistil. cn, Chalazal nucleus; fm, functional megaspore; mmc, megaspore mother cell; mn, micropylar nucleus. Two overlapping high-magnification images were taken for one pistil. The images were then overlaid with Photoshop (Adobe) to show the whole pistil. Bars = 2 μm for **(A)** to **(D)**, 10 μm for **(E)** to **(H)**, 100 μm for **(I)**.

KETCH1 Interacts with RPs

Because KETCH1 is an importin, the roles it plays are most likely conferred by its cargos. Phylogenetic analysis indicated that Arabidopsis KETCH1 is closely related to mammalian importin 5 (IPO5; Zhang et al., 2017), which mediates the nuclear import of several RPs in mammals (Jäkel and Görlich, 1998). We first examined whether KETCH1 interacts with these RP homologs by bimolecular fluorescence complementation (BiFC). Among the RPs whose homologs are cargos of mammalian IPO5, RPL23A, RPS7, RPS3A, and RPL27a, but not RPL5 or RPL23a, interacted with KETCH1 in the nucleus (Figure 7A; Supplemental Figure 7).

Because RPL27a is required for both gametogenesis and embryogenesis, whose mutants showed similar, albeit less severe, phenotypes as *ketch1-2* (Szakonyi and Byrne, 2011; Zsögön et al., 2014), we further verified its interaction with KETCH1 by in vitro pull-down assays (Figure 7B). The interaction between KETCH1 and RPL27a is specific because importin β4 (IMB4), a close homolog of KETCH1 (Tamura and Hara-Nishimura, 2014) and recently shown to regulate the nucleocytoplasmic shuttling of the transcription coactivator GRF-INTERACTING FACTOR1 (GIF1) in integument cells (Liu et al., 2019), did not interact with RPL27a (Supplemental Figure 7), and nor did GIF1 interact with KETCH1 (Supplemental Figure 7). These results suggest a pairwise specificity between importins and their cargos.

Nuclear Accumulation of RP RPL27a Requires KETCH1

To determine whether KETCH1 mediates the nuclear accumulation of RPL27a, as would be expected if it fulfils the role of an importin, we introduced Pro_{UBQ10}:GFP-RPL27aC into Pro_{UBQ10}:KETCH1-mRFP/+*;ketch1-2*, in which pollen grains with red fluorescent protein (RFP) signals are comparable to those of wild type, whereas pollen grains without RFP signals are of the *ketch1-2* genotype. We examined pollen grains from the Pro_{UBQ10}:GFP-RPL27aC;Pro_{UBQ10}:KETCH1-mRFP/+*;ketch1-2* plants. In all pollen grains with clear RFP signals, there were strong GFP signals mostly in the nucleus (Figure 8A). By contrast, pollen grains without detectable RFP signals contained significantly reduced GFP signals (Figures 8A and 8H). GFP signals, i.e., RPL27a levels, are significantly higher when coexpressed with KETCH1-mRFP, suggesting that the nuclear accumulation of RPL27a depends on KETCH1.

Interestingly, in the meristem and elongating zones of the Pro_{UBQ10}:GFP-RPL27aC transgenic roots, GFP signals could only

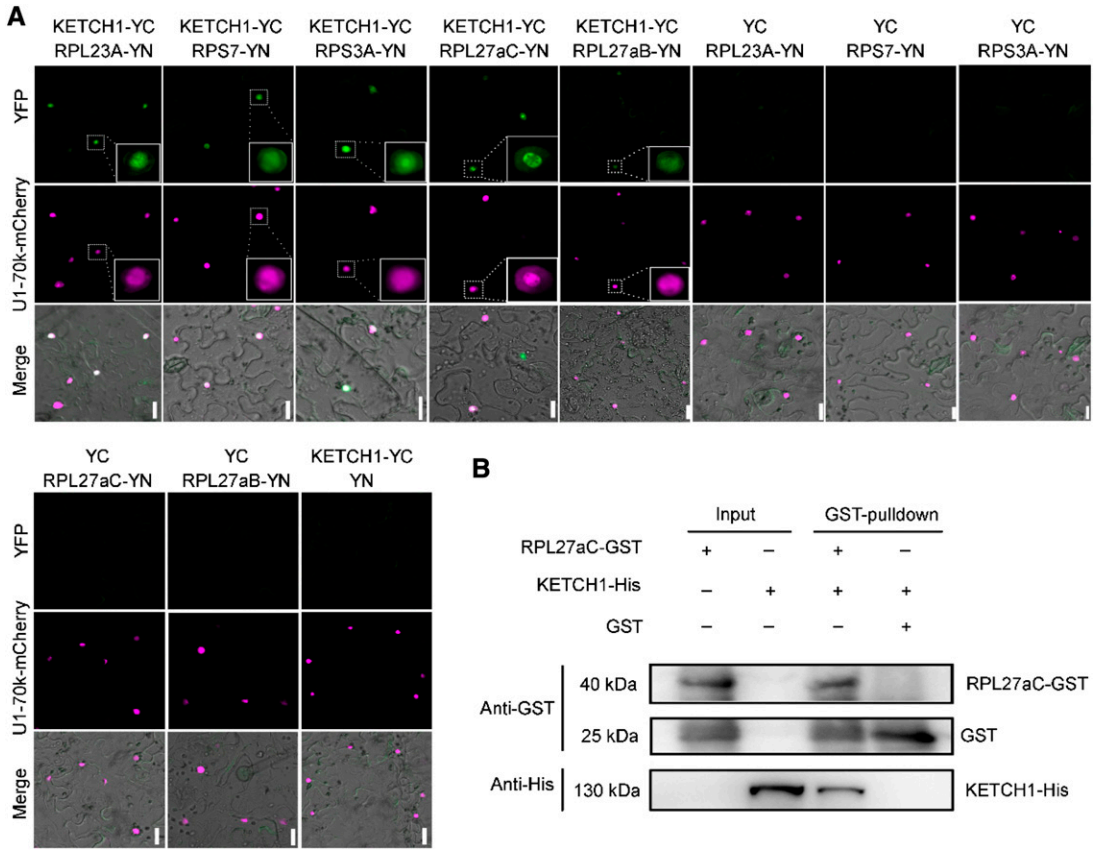

Figure 7. KETCH1 Interacts with Several RPs.

(A) BiFC assays showing the interaction between KETCH1 and several RPs, including RPL23A, RPS7, RPS3A, RPL27aC, and RPL27aB. U1-70k-mCherry was used to label the nucleus and to mark transformed cells. Positive interactions were highlighted as insets. BiFC-positive signals are shown in green while U1-70k-mCherry is in magenta. From top to bottom, the YFP channel, the RFP channel, merges of the YFP, RFP, and transmission channels. For each combination, 30 pavement cells from five tobacco infiltrated leaves were examined with the same results.
(B) In vitro pull-down showing that KETCH1 interacts with RPL27aC. Experiments were performed three times with similar results. Bars = 20 μm.

be detected when MG132, an inhibitor for the 26S proteasome, was added to the medium (Figures 8B, 8C, and 8I). Coexpressing KETCH1-mRFP by Pro_{UBQ10} caused the same effect as MG132 (Figures 8D, 8E, and 8I), indicating that KETCH1 prevents 26S proteasome-mediated RPL27a degradation.

Although the homozygous *ketch1-2* mutant cannot be obtained due to male and female gametophytic defects (Table 1), Pro_{35S}:amiR-KETCH1 plants (amiR) that were generated previously showed reduced leaf size and morphology (Zhang et al., 2017), similar to that shown by the mutants of several RP-coding genes (Byrne, 2009; Rosado et al., 2012; Carroll, 2013). We thus used the amiR plants (Zhang et al., 2017) to examine whether down-regulating *KETCH1* affected the nuclear accumulation of RPL27a also in leaves. By examining the abaxial epidermal cells of Pro_{35S}:amiR-KETCH1;Pro_{UBQ10}:GFP-RPL27aC leaves, we confirmed that down-regulating *KETCH1* significantly reduced the nuclear accumulation of RPL27a in leaf protoplasts and pavement cells (Figures 8F, 8G, 8J, and 8K), similar to that in pollen grains. Two other RPs that interact with KETCH1, i.e., RPL23A and RPS3A, were also significantly reduced in their nuclear accumulation, similar to that of RPL27a (Supplemental Figure 8). By contrast, GIF1, the interactor and cargo of IMB4 (Liu et al., 2019), did not differ in its nuclear accumulation between wild type and Pro_{35S}:amiR-KETCH1 (Supplemental Figure 8). These results showed that KETCH1 positively regulates the nuclear accumulation of its interacting RPs.

Down-regulating *KETCH1* Caused Reduced Ribosome Biogenesis and Translational Efficiency

Because KETCH1 is required for the nuclear accumulation of its interacting RPs (Figure 8; Supplemental Figure 8), we wondered whether ribosome biogenesis and translational capacity would be affected by KETCH1. To test this hypothesis, we first performed polysome profiling assays in the Pro_{35S}:amiR-KETCH1 plants to determine whether down-regulating *KETCH1* could affect ribosome biogenesis. Indeed, the Pro_{35S}:amiR-KETCH1 plants showed a clear reduction in both 40S and 80S subunit intensity peaks to those in the wild type (Figure 9A), suggesting reduced ribosome biogenesis by down-regulating *KETCH1*.

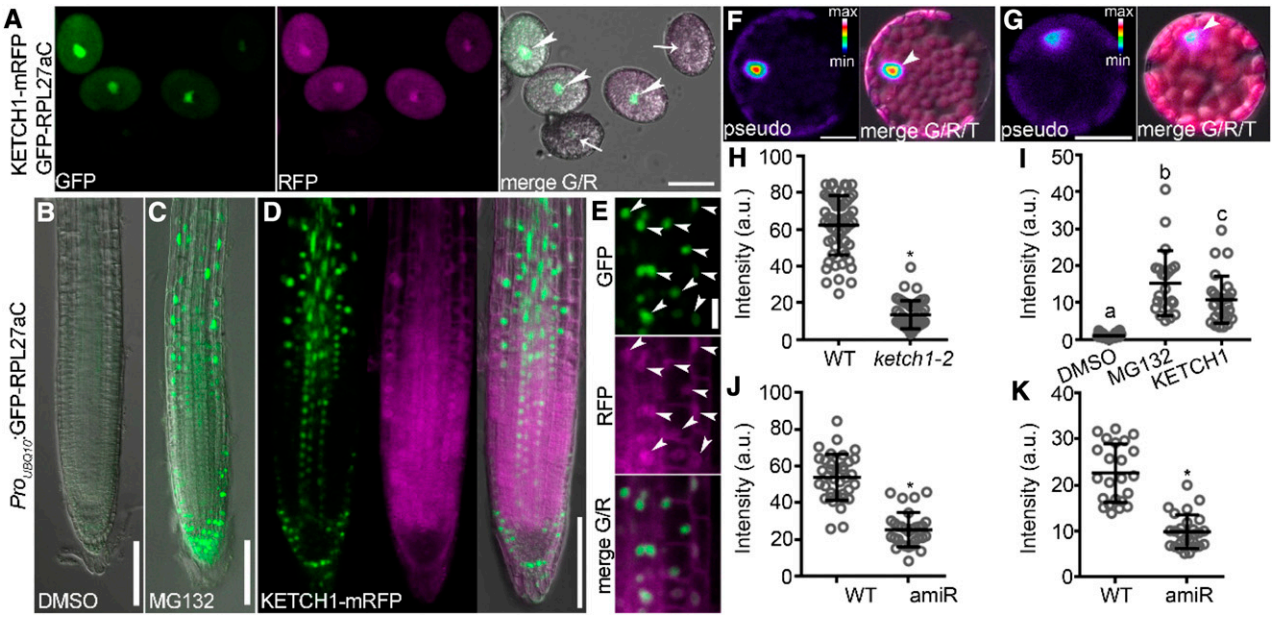

Figure 8. *KETCH1* Positively Regulates the Nuclear Accumulation of RPL27a.

(A) Pollen grains from the Pro_{UBQ10}:GFP-RPL27aC;Pro_{UBQ10}:KETCH1-mRFP/-;*ketch1-2* plants. Arrowheads point at the nuclei of pollen grains expressing GFP-RPL27aC (green) and KETCH1-mRFP (magenta); arrows point at the nuclei of pollen grains with weak or undetectable signals of GFP-RPL27aC and KETCH1-mRFP. Images are Z-stacks of eight confocal sections.

(B) and **(C)** A representative primary root from the Pro_{UBQ10}:GFP-RPL27aC plants treated with either DMSO **(B)** or MG132 **(C)**. The images shown are merges of the GFP and transmission channels.

(D) A representative primary root from the Pro_{UBQ10}:GFP-RPL27aC;Pro_{UBQ10}:KETCH1-mRFP plants. From left to right, CLSM of the GFP channel, the RFP channel, and merges of the GFP, RFP, and transmission channels. Confocal imaging of the GFP channel was performed with the same settings for **(B)** to **(D)**.

(E) Closeup of the images in **(D)**. From top to bottom, CLSM of the GFP channel, the RFP channel, and the merge of the GFP and RFP channels. Arrowheads point to the nuclei with both GFP and RFP signals.

(F) and **(G)** A leaf protoplast from the Pro_{UBQ10}:GFP-RPL27aC **(F)** or Pro_{UBQ10}:GFP-RPL27aC;Pro_{35S}:amiR-KETCH1 plants **(G)**. Confocal imaging was performed with the same settings. Left, CLSM of the GFP channel; right, the merge of the GFP channel, autofluorescence from chlorophyll, and the transmission channel. For GFP signals, intensities are represented in pseudo-color, covering the full range of measured values within each data set (min to max). Arrowheads point at the nuclei.

(H) Intensity of nuclear-associated GFP in pollen grains expressing both KETCH1-mRFP and GFP-RPL27aC (wild type [WT]) or those without clear RFP signals (*ketch1-2*).

(I) Intensity of nuclear-associated GFP in the Pro_{UBQ10}:GFP-RPL27aC transgenic roots, either treated with DMSO, with MG132, or coexpressing KETCH1.

(J) and **(K)** Intensity of nuclear-associated GFP in leaf protoplasts **(J)** or leaf abaxial epidermal cells **(K)** of the Pro_{UBQ10}:GFP-RPL27aC (WT) or Pro_{UBQ10}:GFP-RPL27aC;Pro_{35S}:amiR-KETCH1 (amiR) transgenic plants. a.u. represents arbitrary fluorescence unit. Results in **(H)** to **(K)** are means ± SD ($n > 23$). Asterisks in **(H)**, **(J)**, **(K)** indicate significant difference (*t* test, $P < 0.05$). Different letters in **(I)** indicate significantly different groups (one-way ANOVA, Tukey's multiple comparisons test, $t < 0.05$). Bars = 20 μm for **(A)**, **(E)**, **(F)**, and **(G)**, 100 μm for **(B)** to **(D)**.

Next, we examined the translational capacity in the Pro_{35S}:amiR-KETCH1 plants. Genes with an upstream open reading frame (uORF) located on their 5′ leader sequences are sensitive to translational efficiency (Fernandez et al., 2005), among which *AUXIN RESPONSE FACTOR2* (*ARF2*) and *ARF3* were shown to be affected translationally in the mutants of RPs (Rosado et al., 2012). We thus generated a transgenic line expressing a GFP translational fusion of *ARF2* and *ARF3* with their corresponding uORF into either wild-type or the Pro_{35S}:amiR-KETCH1 protoplasts. The promoter Pro_{UBQ10} was used to exclude the influence of transcription (Supplemental Figure 9). As shown in Figure 9, translational repression, as indicated by reduced GFP signals for either *ARF2* or *ARF3* with uORF, was detected in the Pro_{35S}:amiR-KETCH1 protoplasts compared with their respective controls in wild type (Figures 9B to 9D). By contrast, GFP-fusion proteins translated from *ARF2* or *ARF3* without uORF did not significantly differ between wild type and amiR-KETCH1 (Supplemental Figure 9). These results suggest that KETCH1 positively regulates ribosome biogenesis and translational efficiency, likely by maintaining the nuclear accumulation of RPs.

Because functional loss of *KETCH1* resulted in mitotic arrest during gametogenesis (Figures 3 and 4) and ribosome biogenesis is involved in cell cycle progression in yeast and mammals (Dez and Tollervey, 2004; Donati et al., 2012), we considered the possibility that KETCH1 may indirectly mediate cell cycle progression since it positively regulates ribosome biogenesis via RPs. To test this hypothesis, we examined cell size and contents of leaf epidermal cells. Compared to those of wild type, Pro_{35S}:amiR-KETCH1 contained larger pavement cells (Figures 10A and 10E) and reduced cell density (Figures 10C and 10D), as would be

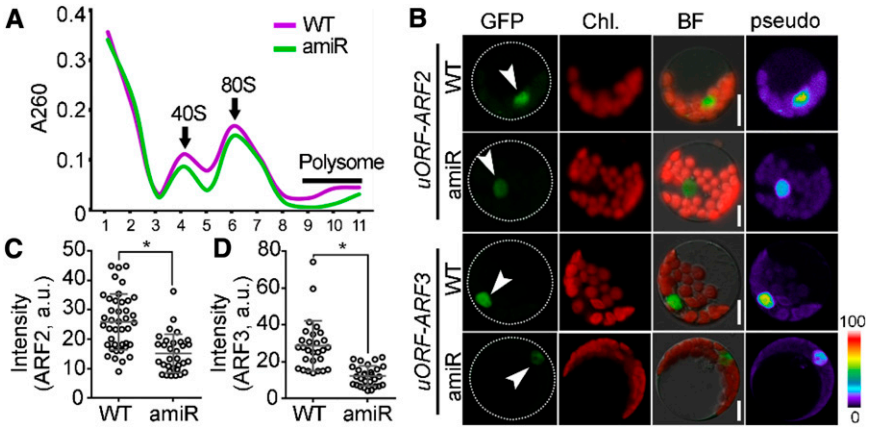

Figure 9. Down-regulating *KETCH1* Reduced Ribosomal Biogenesis and Translational Efficiency.

(A) Polysome profiling assay with sucrose density gradient. The OD260 absorption (A260) was monitored together with fractionation. The fractions containing 40S, 80S of ribosome, and polysomes in wild type (WT) or Pro_{35S}:amiR-KETCH1 (amiR) are indicated. Three biological replicates were performed, and similar results were obtained.

(B) CLSM of a GFP-translational fusion of ARF2 or ARF3 from wild-type or Pro_{35S}:amiR-KETCH1 protoplasts transformed with Pro_{UBQ10}:*uORF-ARF2-GFP* or Pro_{UBQ10}:*uORF-ARF3-GFP*. Dotted lines illustrate protoplast silhouettes and arrowheads point at the nuclei.

(C) and **(D)** GFP intensity in the nucleus for ARF2 **(C)** or ARF3 **(D)** from wild-type or Pro_{35S}:amiR-KETCH1 protoplasts transformed with Pro_{UBQ10}:*uORF-ARF2-GFP* or Pro_{UBQ10}:*uORF-ARF3-GFP*. a.u., Arbitrary fluorescence unit. Results are means ± SD ($n > 28$) from two batches of transformation events. Asterisks indicate significant difference (*t* test, $P < 0.05$). Bars = 10 μm.

expected if cell cycle progression is delayed (Yang et al., 2019). 4′,6-diamidino-2-phenylindole (DAPI) staining of leaf epidermal cells further showed that a larger percentage of cells from the Pro_{35S}:amiR-KETCH1 plants showed either 4C or 8C DNA content than those from wild type (Figure 10F). These results indicate that the expression of *amiR-KETCH1* compromised cell cycle progression.

Discussion

In this report, we demonstrate that *KETCH1* is critical for both male gametogenesis and FG. Although *KETCH1* is also required for embryogenesis (Zhang et al., 2017), several lines of evidence supported a critical role of *KETCH1* in gametogenesis. First, male and female gametophytic transmission of *ketch1-2* was severely reduced (Table 1). Second, reciprocal crosses using the heterozygous *ketch1-2*/+ as the female parent resulted in reduced seed set, similar to that of self-fertilized *ketch1-2*/+ (Figure 1). Third, the development of pollen and embryo sac were defective (Figures 2 to 4). Defective embryo sac development caused reduced pollen tube attraction, leading to partial female sterility (Figure 5). *KETCH1* is expressed throughout male gametogenesis and FG (Figure 6), consistent with its roles in these processes.

The developmental function of KETCH1 is presumably performed through regulating its cargoes. Although HYL1 was shown to be a cargo of KETCH1 (Zhang et al., 2017), reciprocal crosses together with segregation ratio analysis of *hyl1-2*, a null mutant of *HYL1*, indicated that male and female gametophytic transmission was not affected in *hyl1-2* (Supplemental Table 1). Instead, we show that RPL27a and a few other RPs interact specifically with KETCH1 (Figure 7; Supplemental Figure 7). Furthermore, the nuclear accumulation of RPL27a was significantly reduced in pollen grains and other cell types of *ketch1-2* or by down-regulating *KETCH1* (Figure 8; Supplemental Figure 8), suggesting that RPL27a and likely other RPs with which it interacts are also cargos of KETCH1. Among these KETCH1-interacting RPs, RPL27a is critical for gametophytic transmission (Szakonyi and Byrne, 2011; Zsögön et al., 2014), whose reduced nuclear accumulation in *ketch1-2* may have contributed to its gametophytic lethality. On the other hand, down-regulating *KETCH1* constitutively caused altered leaf morphology (Zhang et al., 2017), similar to that caused by mutations at *RPL27aC* or *RPL23A* (Degenhardt and Bonham-Smith, 2008; Szakonyi and Byrne, 2011), hinting at a genetic link between KETCH1 and its interacting RPs.

The interaction with KETCH1 may protect RPs from 26S proteasome-mediated degradation. In mammals, RPs, such as RPL27a, are rapidly degraded in the nucleus to balance a certain rate of ribosome-subunit production (Lam et al., 2007). Such a degradation depends on the 26S proteasome (Sung et al., 2016). Our data suggest a similar regulation in plants. Inhibiting the 26S proteasome by MG132 significantly increased the protein level of RPL27a, which was otherwise undetectable (Figure 8). Coexpression of KETCH1 showed the same effect as did MG132 on RPL27a (Figure 8), suggesting a protective role of KETCH1 through interaction. It has been demonstrated recently that IMB4 positively regulates the turnover of a Kinesin-4 (Ganguly et al., 2018), suggesting that importin-mediated protein stability against the 26S proteasome may be a common theme in plant cells.

Both the large and small subunits of the eukaryotic ribosome assemble in the nucleus (Byrne, 2009). Thus, reduced nuclear accumulation of RPs would compromise ribosomal biogenesis. This was indeed the case when *KETCH1* was down-regulated (Figure 9). Consequently, translational capacity, indicated by the expression of uORF-containing *ARF2* and *ARF3*, was reduced

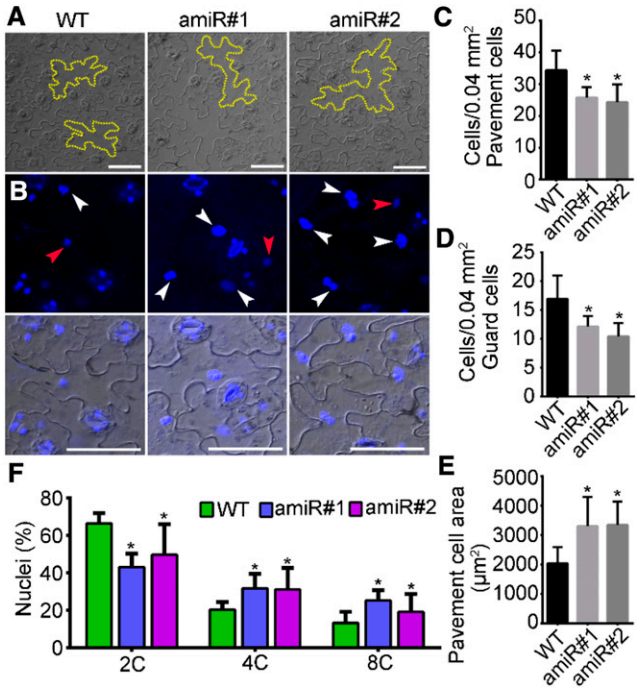

Figure 10. The Expression of *amiR-KETCH1* Compromised Cell Cycle Progression.

(A) Pavement cells from the wild type (WT) and two lines of Pro_{35S}:amiR-KETCH1 (amiR#1 and amiR#2) after tissue clearing. Dotted lines illustrate the morphology of pavement cells.

(B) CLSM of DAPI-stained leaf epidermal cells from wild type, amiR#1, and amiR#2. Red arrowheads point at 2C nuclei, whereas white arrowheads points at nuclei with 4C or 8C (DNA contents).

(C) and **(E)** Quantification of the density **(C)** and **(D)** and the size **(E)** of leaf epidermal cells. Results shown are means ± SD ($n = 10$). Asterisks indicate significant difference from that of wild type (*t* test, $P < 0.05$).

(F) Percentage of nuclei either with 2C, 4C, or 8C DNA content. Results shown are means ± SE ($n = 3$). Asterisks indicate significant difference from that of wild type (*t* test, $P < 0.05$). More than 100 cells from three leaves of three individual plants were analyzed. Bars = 50 μm for **(A)** and **(B)**.

(Figure 9). It was proposed that cells might monitor their translational capacity to determine cell cycle progression, whereas mutations affecting ribosome biogenesis would prevent cells at the G1/S boundary, leading to mitotic cell cycle arrest (Dez and Tollervey, 2004; Donati et al., 2012). In addition, a study in mammals indicated that a delay of cell cycle progression may occur before any detectable difference on ribosome number or translation when an rRNA processing factor was depleted (Bernstein et al., 2007), suggesting that cells sense some aspect of ribosome biogenesis in order to control cell cycle progression. Because male gametogenesis and FG were arrested right before mitosis by *KETCH1* loss of function (Figures 3 and 4), it was a tempting thought that reduced nuclear accumulation of RPs in *ketch1-2* results in the arrest of mitotic cell division during gametogenesis, which was supported by the observation that the amiR-KETCH1 plants show reduced mitotic division in leaf epidermal cells (Figure 10). Whether this reduction was due to a general reduction of protein translation or to some specific component(s) merits further investigation.

A large portion of proteins are required in the nucleus, sometimes dynamically, once they have been synthesized in the cytoplasm. By contrast, only dozens of importins are encoded in a genome such as that of Arabidopsis (Tamura and Hara-Nishimura, 2014). Thus, the cargo specificity of importins has often been questioned. However, our data unequivocally demonstrated pairwise specificity between importins and cargos (Figure 7; Supplemental Figure 7). That one importin regulates multiple cargos, such as KETCH1 for HYL1 and several RPs, is a solution for this dilemma. Identifying consensus motifs that are responsible for the interaction with individual importins, if possible, will be a rewarding effort in the future.

METHODS

Plant Growth and Transformation

The T-DNA insertion line SALK_050129 (*ketch1-2*) was obtained from the Arabidopsis Biological Resource Center (www.arabidopsis.org). The Arabidopsis (*Arabidopsis thaliana*) Columbia-0 ecotype was used as the wild type. Plants were grown in nutrient-rich soil in greenhouse with normal light conditions (90 μmol/m^2/s) at a long-day cycle (16 h light/8 h dark) at 22°C as described by Zhou et al. (2013). Stable transgenic plants were selected on half-strength Murashige and Skoog medium supplemented with 30 μg/mL Basta salts (Sigma-Aldrich) or 25 μg/ml hygromycin (Roche). Other materials, including *hyl1-2* (Lu and Fedoroff, 2000), Pro_{35S}:amiR-KETCH1 (Zhang et al., 2017), Pro_{LAT52}:GUS (Li et al., 2013), Pro_{DD45}:GUS (Wang et al., 2016), and Pro_{ES1}:NLS-YFP (Wang et al., 2017), were described previously.

DNA Manipulation

All constructs were generated using the Gateway technology (Invitrogen). All entry vectors were generated in the pENTR/D/TOPO vector (Invitrogen). The promoter for *KETCH1* was cloned with the primer pair ZP4211/ZP4212 from Columbia-0 genomic DNA. Pro_{KETCH1} containing the 2135-bp sequence upstream of its start codon was introduced into the destination vectors GW:NLS-YFP (Wang et al., 2013) and GW:GUS (Zhou et al., 2013). The full-length coding sequence of *KETCH1*, *RPL27aC*, *RPL27aB*, *RPS3A*, *RPL23A*, *RPS7*, *RPL5*, and *RPL23a* was cloned using the primer pairs ZP4213/ZP4214, ZP7265/ZP7266, ZP8964/ZP8965, ZP8948/ZP8949, ZP7524/ZP7525, ZP8942/ZP8943, ZP8944/ZP8945, and ZP7504/ZP7505, respectively. The uORF for *ARF2* or *ARF3* (Rosado et al., 2012) was cloned using the primer pairs ZP9771/ZP9772 and ZP9773/ZP9774, respectively. The full-length coding sequence of *ARF2* or *ARF3* without uORF was cloned using the primer pairs ZP9772/ZP11174 and ZP9774/ZP11175, respectively. The entry vectors were used in LR reactions with the destination vector Pro_{UBQ10}:GW-YFP to generate Pro_{UBQ10}:*ARF2*-YFP or Pro_{UBQ10}:*ARF3*-YFP.

To generate the destination vector used in in planta protein expression, Pro_{UBQ10}:GW-YFP, Pro_{UBQ10}:GW-RFP, Pro_{35S} of the destination vector Pro_{35S}:GW-YFP, or Pro_{35S}:GW-RFP (Karimi et al., 2002) was replaced with Pro_{UBQ10}, which was amplified with the primer pair ZP510/ZP511 and digested with *Hind*III/*Spe*I. Expression vectors were generated by LR reactions using Gateway LR Clonase II (Invitrogen).

For the KETCH1-RNAi construct, a 490-bp fragment of the *KETCH1* coding sequence (from 1 bp to 490 bp starting from the start codon) was amplified with the primer pair ZP5338/ZP5339. The resulting PCR products were subcloned into the RNAi vector pTCK303 (Guo et al., 2010) to obtain the Pro_{35S}:KETCH1-RNAi construct. The construct Pro_{GPR1}:KETCH1-RNAi

was generated by cloning the promoter of GPR1 (Pro_{GPR1}; Yang et al., 2017) with ZP9474/ZP9475 and replacing Pro_{35S} in Pro_{35S}:KETCH1-RNAi.

Constructs used in BiFC assays were generated with entry vectors and the destination vector pSITE::cEYFP-C1 or pSITE-nEYFP-C1 (Martin et al., 2009) by LR reactions. BiFC constructs for IMB4 or GIF1 were described by Liu et al. (2019). For constructs used for protein expression in the pull-down assay, the coding sequence of *RPL27aC* was inserted into pGEX4T-1 to obtain a vector expressing the recombinant protein glutathione S-transferase (GST)-RPL27aC while the coding sequence of *KETCH1* was inserted into pET30a to obtain a vector expressing the recombinant protein 6× His-KETCH1.

All PCR amplifications were performed using Phusion hot-start high-fidelity DNA polymerase using the annealing temperature and extension times recommended by the manufacturer (Finnzyme). All entry vectors were sequenced, and sequences were analyzed using VectorNTI (Invitrogen). The Bioneer PCR purification kit and the Bioneer Spin miniprep kit were used for PCR product recovery and plasmid DNA extraction, respectively. All primers are listed in Supplemental Table 2.

RNA Extraction, RT-PCRs, and qPCRs

The genotypes of *ketch1-2*/+ progenies were determined by PCRs using the following primers: ZP4148/ZP4149 for *KETCH1* and ZP1/ZP4148 for *ketch1-2*. The genotype of *qrt1* was determined by examining mature pollen.

Total RNAs were isolated using a Qiagen RNeasy plant mini kit according to the manufacturer's instructions. Oligo(dT)-primed cDNAs were synthesized using SuperScript III reverse transcriptase with on-column DNase digestion (Invitrogen). For RT-PCR analysis of complementation lines, the endogenous or exogenous *KETCH1* was amplified with the primer pair ZP5720/ZP4214 or ZP11/ZP4148, respectively. Primers to amplify *ACTIN2* were as described by Zhou et al. (2013).

The qPCRs were performed with the Bio-Rad CFX96 real-time system using SYBR green real-time PCR master mix (Toyobo) as described by Zhou et al. (2013). Primers used in qPCRs were ZP4494/ZP4495 for *KETCH1*, ZP7994/ZP7995 for *RPL27aC*, ZP9772/GFP-F for *ARF2-GFP*, and ZP9774/GFP-F for *ARF3-GFP*. Primers for *GAPDH* and *ACTIN2* in qPCRs were as described by Zhou et al. (2013). All primers are listed in Supplemental Table 2.

Phenotypic Analysis

Methods to analyze pollen development, including Alexander staining, DAPI staining, or SEM, were performed as described by Li et al. (2013) and Feng et al. (2016). Semithin sections and TEM of developing anthers were performed as described by Xie et al. (2014), Feng et al. (2017a), and Zhang et al. (2018). Arabidopsis in vitro pollen tube growth was performed as described by Boavida and McCormick (2007). Whole-mount ovule clearing, optical sections of developing flowers, and SEM were performed as described by Wang et al. (2016, 2017) and Liu et al. (2019). Histochemical GUS analysis of Pro_{LAT52}:GUS-pollinated pistils and aniline blue staining of pollinated pistils were performed as described by Li et al. (2013) and Feng et al. (2018). Measurement of epidermal cell size and density was conducted as described by Horváth et al. (2006). Cells were photographed from at least three different positions of a leaf, and on average 50 cells were analyzed per genotype. Cell outlines were traced and parameters such as cell area, perimeter, and shape factor were calculated with ImageJ (http://rsbweb.nih.gov/ij/). The analysis of DNA content was described previously by Yang et al. (2019). In brief, leaves were dissected and fixed in 70% ethanol for 3 h and then incubated in DAPI staining solution for at least 20 min before imaging. The total integrated density of DAPI fluorescence from selected nuclei was measured.

BiFC Assays

BiFC assays, in which a P19 protein was used to suppress gene silencing (Park et al., 2014), were performed as described by Li et al. (2018b) and Liu et al. (2019). U1-70K-mCherry was used to label the nucleus as described by Wang et al. (2012). Confocal imaging was performed 48 h after tobacco (*Nicotiana tabacum*) leaf infiltration.

Protein Biochemical Assays

For the purification of recombinant proteins in in vitro pull-down assays, pET30a-KETCH1 and GST-RPL27aC were transformed into BL21 competent cells (DE3). The BL21 cells were grown at 37°C in Lurani-Bertani medium in the presence of antibiotics (100 μg/mL kanamycin) to an OD_{600} of 0.6 to 0.8. Protein expression was induced by adding isopropyl-β-D-1-thiogalactopyranosid to a final concentration of 0.5 mM. Cells were further incubated in a horizontal shaker with slow shaking overnight at 16°C before pellet collection by centrifugation at 13,800*g* for 10 min at 4°C. Cell pellets were resuspended and lysed by sonification on ice in a lysis buffer (20 mM Tris·HCl, pH 7.5, 300 mM NaCl, 2 mM phenylmethylsulfonyl fluoride). Supernatant was centrifuged at 16,000*g* for 30 min at 4°C to completely remove cell debris. The 6× His-KETCH1 or GST-RPL27aC recombinant proteins were purified using an Ni-NTA column or glutathione agarose beads, respectively (Zhang et al., 2017).

In vitro pull-down assays were performed as described by Wang et al. (2016). Approximately 1 μg each of GST or GST-RPL27aC proteins was bound to 45 μL of glutathione sepharose beads for 1 h at 4°C. Bound beads were incubated with 1 μg of 6× His-KETCH1 proteins for another 1 h at 4°C. After three washes with 1× PBS buffer, the beads were eluted with 40 μL of 10 mM glutathione in 50 mM Tris (pH 8.0), mixed with a loading buffer, and then boiled at 100°C for 10 min. Approximately 15 μL of each boiled sample was used for SDS-PAGE and protein gel-blot analysis with an anti-His antibody (Beyotime, cat. no. AF5060, 1:1000 dilution) and an anti-GST antibody (Beyotime, cat. No. AF0174, 1:1000 dilution).

Polysome Profiling

Polysome profiling was performed as described by Li et al. (2018a). In brief, leaves from 15-d-old wild-type or Pro_{35S}:amiR-KETCH1 plants were ground in liquid nitrogen, followed by resuspension in polysome extraction buffer. The extract was loaded onto a 10% to 60% Suc gradient and spun in a Hitachi CP100WX/CR22N at 30,000 rpm for 4 h at 4°C. Eleven fractions were collected into centrifugal tubes. The 40S and 80S of ribosome and polysomes were quantified by OD_{260} absorbance profile.

Analysis of DNA Content

For DAPI staining of nuclei, abaxial epidermal cells of the third true leaf from 3 week after germination plants were used for analysis. Areas of epidermis were chosen near the center of the leaf but away from veins. The analysis of DNA content was described previously (Yang et al., 2019). In brief, leaves were dissected and fixed in 70% ethanol for 3 h, and then incubated in DAPI staining solution for at least 20 min before imaging. The total integrated density of DAPI fluorescence from selected nuclei was measured.

Protoplast Preparation

Arabidopsis protoplasts were prepared according to a previous report (Wang et al., 2017). Three independent experiments involving at least 50 protoplasts were conducted to ensure reproducibility of the results.

Fluorescence Microscopy and Pharmacological Treatment

Staining of tissues with FM4-64 (Wang et al., 2013; Zhang et al., 2015; Chai et al., 2016; Feng et al., 2017b; Wan et al., 2017b) or Lysotracker red (Wang et al., 2016) was as described. For MG132 treatment, plant materials were treated with 100 μM MG132 for 0.5 h before examination. Fluorescent images were captured using a LSM 880 CLSM (Zeiss) with a 40/1.3 oil objective. YFP-RFP double-labeled plant materials were captured alternately using line-switching with the multitrack function (514 nm for YFP and 561 nm for RFP). Fluorescence was detected using a 520- to 550-nm band-pass filter for YFP or a 575- to 650-nm band-pass filter for RFP. Images were processed with an LSM image processing software (Zeiss). For the quantification of fluorescence intensity between nuclear and cytoplasmic fractions, a region of interest of the same size was defined either in the nucleus (Nuc) or cytoplasm (Cyt) within a pollen tube or protoplast. The ratio of fluorescence intensity between the nuclear and cytoplasmic ROS (Chai et al., 2016; Wan et al., 2017a) was calculated using ImageJ (http://rsbweb.nih.gov/ij/).

Statistical Analysis

Quantification data were analyzed using GraphPad Prism 6.02 (www.graphpad.com/scientific-software/prism/). All statistical analyses, one-way ANOVA (Tukey's multiple comparisons test), and *t* test were performed with built-in analysis tools and parameters.

Accession Numbers

Arabidopsis Genome Initiative locus identifiers for the genes mentioned in this article are At5g62000 for *ARF2*; At2g33860 for *ARF3*; At5g19820 for *KETCH1/IMP3*; At1g09700 for *HYL1*; At4g27640 for *IMB4*; At5g28640 for *GIF1/AN3*; At3g23860 for *GPR1*; At1g70600 for *RPL27aC*; At1g23290 for *RPL27aB*; At1g04480 for *RPL23A*; At5g39740 for *RPL5*; At2g39460 for *RPL23a*; At4g34670 for *RPS3A*; At3g02560 for *RPS7*.

Supplemental Data

The following materials are available in the online version of this article.

Supplemental Figure 1. In vitro pollen germination was reduced by *KETCH1* loss of function

Supplemental Figure 2. *KETCH1* loss of function compromised PMI during pollen development

Supplemental Figure 3. Knocking down *KETCH1* by Pro_{GPR1}: KETCH1-RNAi mimicked the fertility defects of *ketch1-2*/+

Supplemental Figure 4. *KETCH1* is constitutively expressed

Supplemental Figure 5. Complementation of *ketch1-2* by Pro_{UBQ10}: KETCH1-YFP

Supplemental Figure 6. KETCH1 is distributed both in the cytoplasm and in the nucleus

Supplemental Figure 7. The interaction between KETCH1 and RPL27a is specific

Supplemental Figure 8. *KETCH1* positively regulates the nuclear accumulation of its interacting RPs

Supplemental Figure 9. *ARFs* without uORF did not show significant difference of translational efficiency between wild type and amiR-KETCH1

Supplemental Table 1. Male and female transmission of *hyl1-2* was comparable to that of wild type

Supplemental Table 2. Oligos used in this study

ACKNOWLEDGMENTS

We thank Yijun Qi for *hyl1-2*, the ABRC for *ketch1-2*, and Feng Yu for the help with polysome profiling. This work was supported by Natural Science Foundation of China (31871422 and 31625003 to Y.Z.; 31771558 and 31970332 to S.L.). Y.Z.'s laboratory is partially supported by the Tai-Shan Scholar Program by Shandong Provincial Government.

AUTHOR CONTRIBUTIONS

S.L. and Y.Z. conceived and supervised the project; F.X. and C.-Y.D. performed the experiments with the assistance by H.-H.L. and J.-H.W.; Z.-H.Z. contributed materials; Y.Z., S.L., F.X., and C.-Y.D. designed the experiments and analyzed the data; Y.Z. wrote the article with contributions of all the authors.

Received October 9, 2019; revised January 2, 2020; accepted February 21, 2020; published February 21, 2020.

REFERENCES

Bernstein, K.A., Bleichert, F., Bean, J.M., Cross, F.R., and Baserga, S.J. (2007). Ribosome biogenesis is sensed at the Start cell cycle checkpoint. Mol. Biol. Cell **18:** 953–964.

Boavida, L.C., and McCormick, S. (2007). Temperature as a determinant factor for increased and reproducible *in vitro* pollen germination in *Arabidopsis thaliana*. Plant J. **52:** 570–582.

Borg, M., Brownfield, L., and Twell, D. (2009). Male gametophyte development: A molecular perspective. J. Exp. Bot. **60:** 1465–1478.

Byrne, M.E. (2009). A role for the ribosome in development. Trends Plant Sci. **14:** 512–519.

Carroll, A.J. (2013). The *Arabidopsis* cytosolic ribosomal proteome: from form to function. Front Plant Sci **4:** 32.

Chai, S., Ge, F.R., Feng, Q.N., Li, S., and Zhang, Y. (2016). *PLURIPETALA* mediates ROP2 localization and stability in parallel to *SCN1* but synergistically with *TIP1* in root hairs. Plant J. **86:** 413–425.

Cui, Y., Fang, X., and Qi, Y. (2016). TRANSPORTIN1 promotes the association of microRNA with ARGONAUTE1 in Arabidopsis. Plant Cell **28:** 2576–2585.

Degenhardt, R.F., and Bonham-Smith, P.C. (2008). *Arabidopsis* ribosomal proteins RPL23aA and RPL23aB are differentially targeted to the nucleolus and are disparately required for normal development. Plant Physiol. **147:** 128–142.

Dez, C., and Tollervey, D. (2004). Ribosome synthesis meets the cell cycle. Curr. Opin. Microbiol. **7:** 631–637.

Donati, G., Montanaro, L., and Derenzini, M. (2012). Ribosome biogenesis and control of cell proliferation: p53 is not alone. Cancer Res. **72:** 1602–1607.

Drews, G.N., and Yadegari, R. (2002). Development and function of the angiosperm female gametophyte. Annu. Rev. Genet. **36:** 99–124.

Falcone Ferreyra, M.L., Casadevall, R., Luciani, M.D., Pezza, A., and Casati, P. (2013). New evidence for differential roles of l10 ribosomal proteins from Arabidopsis. Plant Physiol. **163:** 378–391.

Falcone Ferreyra, M.L., Pezza, A., Biarc, J., Burlingame, A.L., and Casati, P. (2010). Plant L10 ribosomal proteins have different roles during development and translation under ultraviolet-B stress. Plant Physiol. **153:** 1878–1894.

Feng, C., Wang, J.G., Liu, H.H., Li, S., and Zhang, Y. (2017a). *Arabidopsis* adaptor protein 1G is critical for pollen development. J. Integr. Plant Biol. **59:** 594–599.

Feng, Q.N., Kang, H., Song, S.J., Ge, F.R., Zhang, Y.L., Li, E., Li, S., and Zhang, Y. (2016). Arabidopsis RhoGDIs are critical for cellular homeostasis of pollen tubes. Plant Physiol. **170:** 841–856.

Feng, Q.N., Liang, X., Li, S., and Zhang, Y. (2018). The ADAPTOR PROTEIN-3 complex mediates pollen tube growth by coordinating vacuolar targeting and organization. Plant Physiol. **177:** 216–225.

Feng, Q.N., Zhang, Y., and Li, S. (2017b). Tonoplast targeting of VHA-a3 relies on a Rab5-mediated but Rab7-independent vacuolar trafficking route. J. Integr. Plant Biol. **59:** 230–233.

Fernandez, J., Yaman, I., Huang, C., Liu, H., Lopez, A.B., Komar, A.A., Caprara, M.G., Merrick, W.C., Snider, M.D., Kaufman, R.J., Lamers, W.H., and Hatzoglou, M. (2005). Ribosome stalling regulates IRES-mediated translation in eukaryotes, a parallel to prokaryotic attenuation. Mol. Cell **17:** 405–416.

Francis, K.E., Lam, S.Y., and Copenhaver, G.P. (2006). Separation of Arabidopsis pollen tetrads is regulated by *QUARTET1*, a pectin methylesterase gene. Plant Physiol. **142:** 1004–1013.

Ganguly, A., DeMott, L., Zhu, C., McClosky, D.D., Anderson, C.T., and Dixit, R. (2018). Importin-β directly regulates the motor activity and turnover of a kinesin-4. Dev. Cell **44:** 642–651.e5.

Guo, J., Wang, F., Song, J., Sun, W., and Zhang, X.S. (2010). The expression of *Orysa;CycB1;1* is essential for endosperm formation and causes embryo enlargement in rice. Planta **231:** 293–303.

Harel, A., and Forbes, D.J. (2004). Importin beta: conducting a much larger cellular symphony. Mol. Cell **16:** 319–330.

Horváth, B.M., Magyar, Z., Zhang, Y., Hamburger, A.W., Bakó, L., Visser, R.G., Bachem, C.W., and Bögre, L. (2006). EBP1 regulates organ size through cell growth and proliferation in plants. EMBO J. **25:** 4909–4920.

Huang, C.K., Huang, L.F., Huang, J.J., Wu, S.J., Yeh, C.H., and Lu, C.A. (2010). A DEAD-box protein, AtRH36, is essential for female gametophyte development and is involved in rRNA biogenesis in *Arabidopsis*. Plant Cell Physiol. **51:** 694–706.

Imai, A., Komura, M., Kawano, E., Kuwashiro, Y., and Takahashi, T. (2008). A semi-dominant mutation in the ribosomal protein L10 gene suppresses the dwarf phenotype of the *acl5* mutant in *Arabidopsis thaliana*. Plant J. **56:** 881–890.

Jäkel, S., and Görlich, D. (1998). Importin β, transportin, RanBP5 and RanBP7 mediate nuclear import of ribosomal proteins in mammalian cells. EMBO J. **17:** 4491–4502.

Karimi, M., Inzé, D., and Depicker, A. (2002). GATEWAY vectors for *Agrobacterium*-mediated plant transformation. Trends Plant Sci. **7:** 193–195.

Lam, Y.W., Lamond, A.I., Mann, M., and Andersen, J.S. (2007). Analysis of nucleolar protein dynamics reveals the nuclear degradation of ribosomal proteins. Curr. Biol. **17:** 749–760.

Li, C., Liu, X., Qiang, X., Li, X., Li, X., Zhu, S., Wang, L., Wang, Y., Liao, H., Luan, S., and Yu, F. (2018a). EBP1 nuclear accumulation negatively feeds back on FERONIA-mediated RALF1 signaling. PLoS Biol. **16:** e2006340.

Li, E., Cui, Y., Ge, F.R., Chai, S., Zhang, W.T., Feng, Q.N., Jiang, L., Li, S., and Zhang, Y. (2018b). AGC1.5 kinase phosphorylates RopGEFs to control pollen tube growth. Mol. Plant **11:** 1198–1209.

Li, N., Yuan, L., Liu, N., Shi, D., Li, X., Tang, Z., Liu, J., Sundaresan, V., and Yang, W.C. (2009). *SLOW WALKER2*, a NOC1/MAK21 homologue, is essential for coordinated cell cycle progression during female gametophyte development in Arabidopsis. Plant Physiol. **151:** 1486–1497.

Li, S., Ge, F.R., Xu, M., Zhao, X.Y., Huang, G.Q., Zhou, L.Z., Wang, J.G., Kombrink, A., McCormick, S., Zhang, X.S., and Zhang, Y. (2013). *Arabidopsis* COBRA-LIKE 10, a GPI-anchored protein, mediates directional growth of pollen tubes. Plant J. **74:** 486–497.

Liu, H.H., Xiong, F., Duan, C.Y., Wu, Y.N., Zhang, Y., and Li, S. (2019). Importin β4 mediates nuclear import of GRF-interacting factors to control ovule development in Arabidopsis. Plant Physiol. **179:** 1080–1092.

Liu, J., and Qu, L.J. (2008). Meiotic and mitotic cell cycle mutants involved in gametophyte development in *Arabidopsis*. Mol. Plant **1:** 564–574.

Liu, J., et al. (2008). Targeted degradation of the cyclin-dependent kinase inhibitor ICK4/KRP6 by RING-type E3 ligases is essential for mitotic cell cycle progression during *Arabidopsis* gametogenesis. Plant Cell **20:** 1538–1554.

Liu, M., Shi, D.Q., Yuan, L., Liu, J., and Yang, W.C. (2010). *SLOW WALKER3*, encoding a putative DEAD-box RNA helicase, is essential for female gametogenesis in *Arabidopsis*. J. Integr. Plant Biol. **52:** 817–828.

Lu, C., and Fedoroff, N. (2000). A mutation in the Arabidopsis *HYL1* gene encoding a dsRNA binding protein affects responses to abscisic acid, auxin, and cytokinin. Plant Cell **12:** 2351–2366.

Martin, K., Kopperud, K., Chakrabarty, R., Banerjee, R., Brooks, R., and Goodin, M.M. (2009). Transient expression in *Nicotiana benthamiana* fluorescent marker lines provides enhanced definition of protein localization, movement and interactions *in planta*. Plant J. **59:** 150–162.

McCormick, S. (1993). Male gametophyte development. Plant Cell **5:** 1265–1275.

McCormick, S. (2004). Control of male gametophyte development. Plant Cell **16** (Suppl): S142–S153.

Meier, I., and Brkljacic, J. (2009). The nuclear pore and plant development. Curr. Opin. Plant Biol. **12:** 87–95.

Nowack, M.K., Harashima, H., Dissmeyer, N., Zhao, X., Bouyer, D., Weimer, A.K., De Winter, F., Yang, F., and Schnittger, A. (2012). Genetic framework of cyclin-dependent kinase function in *Arabidopsis*. Dev. Cell **22:** 1030–1040.

Park, S.J., Jiang, K., Tal, L., Yichie, Y., Gar, O., Zamir, D., Eshed, Y., and Lippman, Z.B. (2014). Optimization of crop productivity in tomato using induced mutations in the florigen pathway. Nat. Genet. **46:** 1337–1342.

Rosado, A., Li, R., van de Ven, W., Hsu, E., and Raikhel, N.V. (2012). *Arabidopsis* ribosomal proteins control developmental programs through translational regulation of auxin response factors. Proc. Natl. Acad. Sci. USA **109:** 19537–19544.

Sanders, P.M., Bui, A.Q., Weterings, K., McIntire, K.N., Hsu, Y.-C., Lee, P.Y., Truong, M.T., Beals, T.P., and Goldberg, R.B. (1999). Anther developmental defects in *Arabidopsis thaliana* male-sterile mutants. Sex. Plant Reprod. **11:** 297–322.

Shi, D.Q., Liu, J., Xiang, Y.H., Ye, D., Sundaresan, V., and Yang, W.C. (2005). *SLOW WALKER1*, essential for gametogenesis in Arabidopsis, encodes a WD40 protein involved in 18S ribosomal RNA biogenesis. Plant Cell **17:** 2340–2354.

Steffen, J.G., Kang, I.H., Macfarlane, J., and Drews, G.N. (2007). Identification of genes expressed in the *Arabidopsis* female gametophyte. Plant J. **51:** 281–292.

Sung, M.K., Reitsma, J.M., Sweredoski, M.J., Hess, S., and Deshaies, R.J. (2016). Ribosomal proteins produced in excess are degraded by the ubiquitin-proteasome system. Mol. Biol. Cell **27:** 2642–2652.

Szakonyi, D., and Byrne, M.E. (2011). Ribosomal protein L27a is required for growth and patterning in *Arabidopsis thaliana*. Plant J. **65:** 269–281.

Takatsuka, H., Umeda-Hara, C., and Umeda, M. (2015). Cyclin-dependent kinase-activating kinases CDKD;1 and CDKD;3 are

essential for preserving mitotic activity in *Arabidopsis thaliana*. Plant J. **82:** 1004–1017.

Tamura, K., and Hara-Nishimura, I. (2014). Functional insights of nucleocytoplasmic transport in plants. Front Plant Sci **5:** 118.

Vazquez, F., Gasciolli, V., Crété, P., and Vaucheret, H. (2004). The nuclear dsRNA binding protein HYL1 is required for microRNA accumulation and plant development, but not posttranscriptional transgene silencing. Curr. Biol. **14:** 346–351.

Wan, Z.Y., Chai, S., Ge, F.R., Feng, Q.N., Zhang, Y., and Li, S. (2017b). Arabidopsis PROTEIN S-ACYL TRANSFERASE4 mediates root hair growth. Plant J. **90:** 249–260.

Wan, Z.Y., Zhang, Y., and Li, S. (2017a). Protein S-acyl transferase 4 controls nucleus position during root hair tip growth. Plant Signal. Behav. **12:** e1311438.

Wang, J.G., Feng, C., Liu, H.H., Feng, Q.N., Li, S., and Zhang, Y. (2017). AP1G mediates vacuolar acidification during synergid-controlled pollen tube reception. Proc. Natl. Acad. Sci. USA **114:** E4877–E4883.

Wang, J.G., Feng, C., Liu, H.H., Ge, F.R., Li, S., Li, H.J., and Zhang, Y. (2016). HAPLESS13-mediated trafficking of STRUBBELIG is critical for ovule development in *Arabidopsis*. PLoS Genet. **12:** e1006269.

Wang, J.G., Li, S., Zhao, X.Y., Zhou, L.Z., Huang, G.Q., Feng, C., and Zhang, Y. (2013). HAPLESS13, the Arabidopsis μ1 adaptin, is essential for protein sorting at the trans-Golgi network/early endosome. Plant Physiol. **162:** 1897–1910.

Wang, W., Ye, R., Xin, Y., Fang, X., Li, C., Shi, H., Zhou, X., and Qi, Y. (2011). An importin β protein negatively regulates microRNA activity in Arabidopsis. Plant Cell **23:** 3565–3576.

Wang, X., et al. (2012). SKIP is a component of the spliceosome linking alternative splicing and the circadian clock in Arabidopsis. Plant Cell **24:** 3278–3295.

Xie, H.T., Wan, Z.Y., Li, S., and Zhang, Y. (2014). Spatiotemporal production of reactive oxygen species by NADPH oxidase is critical for tapetal programmed cell death and pollen development in Arabidopsis. Plant Cell **26:** 2007–2023.

Yamamoto, Y., Nishimura, M., Hara-Nishimura, I., and Noguchi, T. (2003). Behavior of vacuoles during microspore and pollen development in *Arabidopsis thaliana*. Plant Cell Physiol. **44:** 1192–1201.

Yang, K., Zhu, L., Wang, H., Jiang, M., Xiao, C., Hu, X., Vanneste, S., Dong, J., and Le, J. (2019). A conserved but plant-specific CDK-mediated regulation of DNA replication protein A2 in the precise control of stomatal terminal division. Proc. Natl. Acad. Sci. USA **116:** 18126–18131.

Yang, X., Zhang, Q., Zhao, K., Luo, Q., Bao, S., Liu, H., and Men, S. (2017). The Arabidopsis *GPR1* gene negatively affects pollen germination, pollen tube growth, and gametophyte senescence. Int. J. Mol. Sci. **18:** 18.

Zhang, W.T., Li, E., Guo, Y.K., Yu, S.X., Wan, Z.Y., Ma, T., Li, S., Hirano, T., Sato, M.H., and Zhang, Y. (2018). Arabidopsis *VAC14* is critical for pollen development through mediating vacuolar organization. Plant Physiol. **177:** 1529–1538.

Zhang, Y.L., Li, E., Feng, Q.N., Zhao, X.Y., Ge, F.R., Zhang, Y., and Li, S. (2015). Protein palmitoylation is critical for the polar growth of root hairs in *Arabidopsis*. BMC Plant Biol. **15:** 50.

Zhang, Z., Guo, X., Ge, C., Ma, Z., Jiang, M., Li, T., Koiwa, H., Yang, S.W., and Zhang, X. (2017). KETCH1 imports HYL1 to nucleus for miRNA biogenesis in *Arabidopsis*. Proc. Natl. Acad. Sci. USA **114:** 4011–4016.

Zhou, L.Z., Li, S., Feng, Q.N., Zhang, Y.L., Zhao, X., Zeng, Y.L., Wang, H., Jiang, L., and Zhang, Y. (2013). Protein S-ACYL Transferase10 is critical for development and salt tolerance in *Arabidopsis*. Plant Cell **25:** 1093–1107.

Zsögön, A., Szakonyi, D., Shi, X., and Byrne, M.E. (2014). Ribosomal protein RPL27a promotes female gametophyte development in a dose-dependent manner. Plant Physiol. **165:** 1133–1143.